APPLICATION OF LOCAL MESHLESS METHOD FOR THE SOLUTION OF TWO TERM TIME FRACTIONAL-ORDER MULTI-DIMENSIONAL PDE ARISING IN HEAT AND MASS TRANSFER

by

Imtiaz AHMAD[a], Hijaz AHMAD[b], Mustafa INC[c,d], Shao-Wen YAO[e*], and Bandar ALMOHSEN[f]

[a] Department of Mathematics, University of Swabi, Khyber Pakhtunkhwa, Pakistan
[b] Department of Basic Sciences, University of Engineering and Technology Peshawar, Khyber Pakhtunkhwa, Pakistan
[c] Department of Mathematics, Firat University, Elazig, Turkey
[d] Department of Medical Research, China Medical University Hospital, China Medical University, Taichung, Taiwan
[e] School of Mathematics and Information Science, Henan Polytechnic University, Jiaozuo, China
[f] Department of Mathematics, College of Science, King Saud University, Riyadh, Saudi Arabia

Original scientific paper
https://doi.org/10.2298/TSCI20S1095A

In this article, we presented an efficient local meshless method for the numerical treatment of two term time fractional-order multi-dimensional diffusion PDE. The demand of meshless techniques increment because of its meshless nature and simplicity of usage in higher dimensions. This technique approximates the solution on set of uniform and scattered nodes. The space derivatives of the models are discretized by the proposed meshless procedure though the time fractional part is discretized by Liouville-Caputo fractional derivative. The numerical results are obtained for 1-, 2- and 3-D cases on rectangular and non-rectangular computational domains which verify the validity, efficiency and accuracy of the method.

Key words: *two term diffusion equation, Liouville-Caputo derivative, Meshless method, radial basis function*

Introduction

Numerous physical problems, particularly heat transfer, occurring in engineering sciences are thrown into time fractional-order PDE. Contrasted with single-term time fractional PDE, the multi-term time fractional PDE are proposed to improve the modelling accuracy in depicting the anomalous diffusion process, modelling different sorts of viscoelastic damping, precisely catching power-law frequency dependence and simulating flow of a fractional Maxwell fluid [1].

The fractional calculus has attracted significant interests in the field of engineering and applied sciences in the last few years. The elementary knowledge of fractional calculus can be found [2]. Fractional differential equations contain derivatives of any complex or real order, being considered as general form of differential equations. The comprehensive

* Corresponding author, e-mail: yaoshaowen@hpu.edu.cn

applications in real world problems are described by fractional PDE and it is found to be an effective tool in interpretation and modelling of numerous problems appear in physics and applied mathematics [3-8].

Recently, a great effort has been expended to develop the exact and approximate behavior of fractional PDE. In this effort several enthusiastic methods have been applied for the solution of fractional PDE such as homotopy analysis method [9, 10], Adomian decomposition method [11], fractional difference method [12], variational iteration method [13-16], homotophy perturbation method [17], Lie symmetry analysis [18], reproducing kernel method [19], Modified variational iteration method [20], meshless methods [21] and Chebychev spectral method [22].

Different types of meshless techniques have been got expansive consideration for tackling diverse kind of PDE model arise in almost all disciplines of engineering. Especially the RBF (RBF) based meshless methods are one of the most popular type among these methods. The meshless methods do not require mesh in the domain. Moreover, the uses of RBF [23] increase advantages and preferences of technique due to this property that the RBF only depend on the Euclidian distance between two points of the spatial domain. According to these facts, meshless methods are known as very flexible and useful mathematical tools which can be applied to high dimensional models with irregular and complicated domains. Meshless collocation technique based on the RBF is one of the very popular strong-form meshless methods which is widely employed to many practical problems [24]. Although the classical meshless collocation method based on the globally supported RBF is known as a very efficient computational technique to deal with complicated and high dimensional PDE, but the method leads to an ill-conditioned and dense system of algebraic equations. In the global meshless method, the RBF are used to obtain the coefficients, so that the derivatives of a function $f(x)$ can be written as a linear combination of the functional values at the predetermined nodes. This numerical scheme is simple and effective. However, the approximation can become unstable as the number of collocation points become large resulting in dense matrices. This leads to ill-conditioning and sensitivity to the shape parameters in the RBF formulation. Unfortunately, this ill-conditioning and computational cost of implementation of the technique will increase dramatically by increasing number of the scattered data points. To ward off these deficiencies, the researchers suggested local meshless methods (LMM) [21-25].

The LMM uses only neighboring collocation points and it does not have the typical ill-conditioning that comes with large dense matrix systems. Additionally, in such RBF based meshless techniques, the proper selection of RBF as well as shape parameter value play a crucial rule in the convergence. Among these RBF, the multiquadric (MQ) is perhaps the most popular that is used in applications. This is due to its high convergence rate and accuracy. Perhaps a disadvantage that the MQ RBF has as compared to the polyharmonic splines is that the accuracy depends on the correct choice of the shape parameter. The same disadvantage applies to the inverse multiquadric (IMQ) and the Gaussian (GA) RBF as well. Finding the appropriate shape parameter is an ongoing research problem. In LMM, the shape parameter does not vary much, which is beneficial in choosing a good value. Another advantage of the local technique is that the accuracy is not compromised by the computational efficiency. Unlike the global approach where it is required to work with a dense matrix, the local technique results in a sparse matrix which can be solved accurately and efficiently. In the recent literature, LMM are used for better numerical approximation of complex PDE models, see [25].

Current research work is devoted to use the LMM for the numerical investigation of two term time fractional-order diffusion model equations up to 3-D. The space derivatives are approximated by the local meshless procedure using the inverse quadric, multiquadric and the Gaussian RBF whereas time fractional part is approximated by using Liouville-Caputo definition. Both rectangular and non-rectangular geometries are considered in numerical experiments.

Consider the unsteady two term time fractional diffusion PDE:

$$a_1 \frac{\partial^\alpha W(\bar{\mathbf{z}},t)}{\partial t^\alpha} + a_2 \frac{\partial^\beta W(\bar{\mathbf{z}},t)}{\partial t^\beta} = \gamma \nabla W(\bar{\mathbf{z}},t) + F(\bar{\mathbf{z}},t) \equiv \mathcal{L} W\,\bar{\mathbf{z}}(,t) \qquad (1)$$
$$\bar{\mathbf{z}} \in \Omega, \quad 0 < \beta \le \alpha \le 1, \quad t > 0$$

with the following initial-boundary conditions:

$$W(\bar{\mathbf{z}},0) = W_0, \quad C(\bar{\mathbf{z}},t) = g(\bar{\mathbf{z}},t), \quad \bar{\mathbf{z}} \in \partial\Omega \qquad (2)$$

where γ is the diffusion coefficient.

Proposed methodology

The LMM [26] is extended to the time fractional convection-diffusion models. The derivatives of $W(\bar{\mathbf{z}}, t)$ are approximated at the centers $\bar{\mathbf{z}}_h$ by the neighborhood of $\bar{\mathbf{z}}_h$, $\{\bar{\mathbf{z}}_{h1}, \bar{\mathbf{z}}_{h2}, \bar{\mathbf{z}}_{h3},..., \bar{\mathbf{z}}_{hn_h}\} \subset \{\bar{\mathbf{z}}_1, \bar{\mathbf{z}}_2,..., \bar{\mathbf{z}}_{N^n}\}$, $n_h \ll N^n$, where $h = 1, 2,...,N^n$. In case of 1-D , $\bar{\mathbf{z}} = x$, for 2-D $\bar{\mathbf{z}} = (x, y)$, and for 3-D case $\bar{\mathbf{z}} = (x, y, z)$ (3D). Now in 1-D case:

$$W^{(m)}(x_h) \approx \sum_{k=1}^{n_h} \lambda_k^{(m)} W(x_{hk}), h = 1, 2, \ldots, N \qquad (3)$$

By substituting RBF $\psi(\|x - x_p\|)$ in eq. (3):

$$\psi^{(m)}(\| x_h - x_p \|) = \sum_{k=1}^{n_h} \lambda_{hk}^{(m)} \psi(\| x_{hk} - x_p \|), \; p = h_1, h_2, \ldots, h_{n_h} \qquad (4)$$

where

$$\psi(\| x_{hk} - x_p \|) = \sqrt{1 + (c \| x_{hk} - x_p \|)^2}$$

in case of MQ RBF, respectively.

Matrix form of eq. (4) can be written:

$$\psi_{n_h}^{(m)} = \boldsymbol{A}_{n_h} \boldsymbol{\lambda}_{n_h}^{(m)} \qquad (5)$$

From eq. (5), we obtain:

$$\boldsymbol{\lambda}_{n_h}^{(m)} = \boldsymbol{A}_{n_h}^{-1} \psi_{n_h}^{(m)} \qquad (6)$$

Equations (3) and (6) implies:

$$W^{(m)}(x_h) = \left[\boldsymbol{\lambda}_{n_h}^{(m)}\right]^T \mathbf{W}_{n_h}, \text{ where } \mathbf{W}_{n_h} = \left[W(x_{h1}), W(x_{h2}), \ldots, W(x_{hn_h})\right]^T$$

In case of 2-D, the derivatives of $W(x, y, t)$ regarding x and y are approximated in the comparative manner:

$$W_x^{(m)}(x_h, y_h) \approx \sum_{k=1}^{n_h} \gamma_k^{(m)} W(x_{hk}, y_{hk}), \; h = 1, 2, \ldots, N^2 \qquad (7)$$

$$W_y^{(m)}\left(x_h, y_h\right) \approx \sum_{k=1}^{n_h} \eta_k^{(m)} W\left(x_{hk}, y_{hk}\right), \quad h = 1, 2, \ldots, N^2 \tag{8}$$

To find out the relating coefficients $\gamma_k^{(m)}$ and $\eta_k^{(m)}$ (k = 1, 2,..., n_h), we continue:

$$\gamma_{n_h}^{(m)} = \boldsymbol{A}_{n_h}^{-1} \boldsymbol{\Phi}_{n_h}^{(m)}, \quad \eta_{n_h}^{(m)} = \boldsymbol{A}_{n_h}^{-1} \boldsymbol{\Phi}_{n_h}^{(m)} \tag{9}$$

The aforementioned technique can be rehashed for 3-D case, *etc*.

The time derivative $[\partial^\alpha W(\bar{\mathbf{z}}, t)]/\partial t^\alpha$ is discretized by using Liouville-Caputo derivative [27]. The Liouville-Caputo fractional derivative for $\alpha \in (0, 1)$:

$$\frac{\partial^\alpha W\left(\bar{\mathbf{z}}, t\right)}{\partial t^\alpha} = \begin{cases} \dfrac{1}{\Gamma\left(1-\alpha\right)} \displaystyle\int_0^t \frac{\partial W\left(\bar{z}, \vartheta\right)}{\partial \vartheta} \left(t-\vartheta\right)^{-\alpha} \mathrm{d}\vartheta, & 0 < \alpha < 1 \\ \dfrac{\partial W\left(\bar{\mathbf{z}}, t\right)}{\partial t}, & \alpha = 1 \end{cases}$$

For the interval $|0, t]$, $Q + 1$ is considered as equally spaced time intervals t_0, t_1,..., t_Q, such that $t_q = q\tau$, n = 0, 1, 2,..., Q,, , τ is the time step and to approximate the time fractional derivative $(q + 1)^{\text{th}}$ time level:

$$\begin{aligned} \frac{\partial^\alpha W\left(\bar{\mathbf{z}}, t_{q+1}\right)}{\partial t^\alpha} &= \frac{1}{\Gamma\left(1-\alpha\right)} \int_0^{t_{q+1}} \frac{\partial W\left(\bar{\mathbf{z}}, \vartheta\right)}{\partial \vartheta} \left(t_{q+1} - \vartheta\right)^{-\alpha} \mathrm{d}\vartheta \\ &\approx \frac{1}{\Gamma\left(1-\alpha\right)} \sum_{s=0}^{q} \int_{s\tau}^{(s+1)\tau} \frac{\partial W\left(\bar{\mathbf{z}}, \vartheta_s\right)}{\partial \vartheta} \left(t_{s+1} - \vartheta\right)^{-\alpha} \mathrm{d}\vartheta \end{aligned}$$

Integration yields:

$$\frac{\partial^\alpha W\left(\bar{\mathbf{z}}, t_{q+1}\right)}{\partial t^\alpha} \approx \begin{cases} a_0 \left(W^{q+1} - W^q\right) + a_0 \displaystyle\sum_{s=1}^{q} b_s \left(W^{q+1-s} - W^{q-s}\right), & q \geq 1 \\ a_0 \left(W^1 - W^0\right), & q = 0 \end{cases}$$

where

$$a_0 = \frac{\tau^{-\alpha}}{\Gamma\left(2-\alpha\right)} \quad \text{and} \quad b_s = (s+1)^{1-\alpha} - s^{1-\alpha}, \quad s = 0, 1, \ldots, q$$

A similar methodology is applied for the discretization of fractional derivative of order β.

Numerical results

In this section, the numerical results of the 1-, 2-, and 3-D two term time fraction diffusion model equations using the proposed LMM. Multiquadric RBF with shape parameter c = 1 are used for space discretization in all numerical simulation using LMM in implicit form unless mentioned explicitly. All numerical experiments are performed using local supported domain n_i = 3, n_i = 5, and n_i = 7 in 1-, 2-, and 3-D case, respectively, additionally the source

functions in each case can be computed easily in the accordance of the corresponding exact solution. All the computations are performed on HP (ProBook) PC Laptop with an Intel(R) Core(TM) i5-4210M CPU 2.60 GHz 2.60 GHz 4 GB RAM. The accuracy is measure through maximum error norm and root mean error norm (RMS) which are defined:

$$\max(\varepsilon) = \max\left(\left|\hat{\mathbb{W}} - W\right|\right), \quad RMS = \sqrt{\frac{\sum_{i=1}^{N}\left(\hat{\mathbb{W}}_i - W_i\right)^2}{N}} \tag{10}$$

where $\hat{\mathbb{W}}$ is exact solution and W is the approximate solution.

Test problem 1

Consider eq. (1) as 1-D two term diffusion equation with $a_1 = a_2 = \gamma = 1$, having exact solution [28, 29]:

$$W(\bar{\mathbf{z}}, t) = \left(1 + t^2\right)\left(x - x^2\right), \quad t \geq 0, \quad x \in [0,1] \tag{11}$$

Initial and boundary conditions can found in accordance to the exact solution.

The numerical results for Test Problem 1 are obtained by the LMM and compared with the results given in [29] which are shown in tab. 1. It clear from the table that the results of the LMM are more accurate than the method given in [29]. Figure 1 shows the numerical results at different time, t, and nodel points, N, which shows that the suggested method gives good accuracy. Figure 2(a) shows the comparison of numerical and exact solution at different time up to $t = 2$ while fig. 2(b) shows the absolute error at different time which is self explanatory.

Table 1. Simulation results using $\tau = 0.01$, $\alpha = 0.75$, and $\beta = 0.2$ for Test problem 1

	$t = 0.1$		$t = 0.5$		$t = 1$	
	LMM ($N = 10$)	[29] ($N = 25$)	LMM ($N = 10$)	[29] ($N = 25$)	LMM (N=10)	[29] (= 25)
max(ε)	$9.2613 \cdot 10^{-5}$	$7.932 \cdot 10^{-5}$	$1.1997 \cdot 10^{-4}$	$1.155 \cdot 10^{-3}$	$1.8183 \cdot 10^{-4}$	$2.758 \cdot 10^{-3}$
RMS	$7.9853 \cdot 10^{-5}$	$5.233 \cdot 10^{-5}$	$1.0713 \cdot 10^{-4}$	$7.870 \cdot 10^{-4}$	$1.5570 \cdot 10^{-4}$	$1.893 \cdot 10^{-3}$

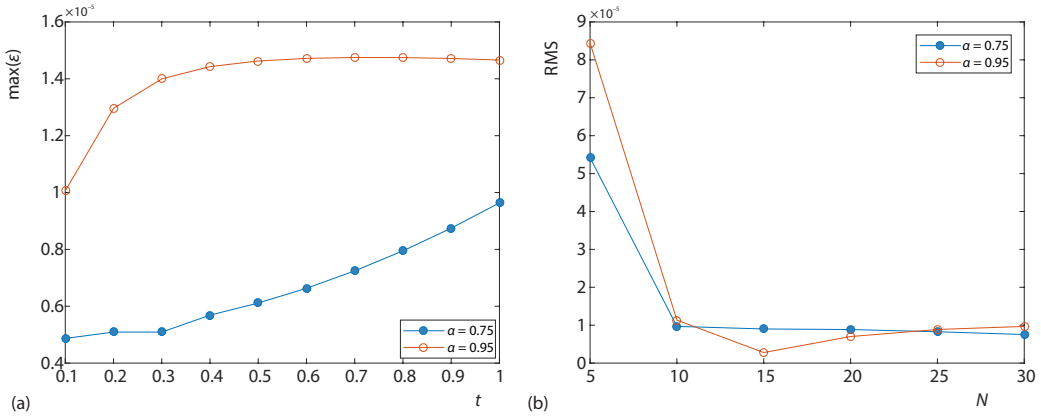

Figure 1. Simulation results using; $N = 32$ (a), $t = 1$ (b) and $\tau = 0.001$, $\beta = 0.2$ for Test problem 1

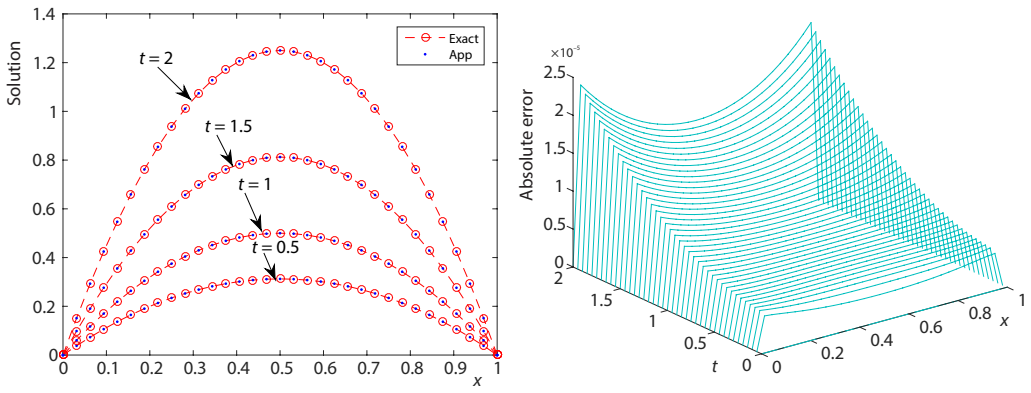

Figure 2. Simulation results using $N = 32$, $\tau = 0.001$, $\alpha = 0.75$, and $\beta = 0.2$ for Test problem 1

Test problem 2

Consider the eq. (1) with $a_1 = a_2 = \gamma = 1$, having exact solution [29] is given as:

$$W(\bar{\mathbf{z}},t) = \sin(\pi x)\sin(\pi y)\exp(-t), \quad t \geq 0 \tag{12}$$

The numerical results for Test problem 2 in terms of max(ε) and RMS norms, are described in tab. 2 using LMM coupled with Crank-Nicolson and implicit method. It can be seen that in this test problem the LMM gives accurate results as compared to the method in [29]. Figure 3 shows the exact, numerical and absolute error for Test problem 2 which is the evidence of the proposed method for better accuracy. Table 3 shows the comparative analysis of the LMM using explicit, Crank-Nicolson and implicit scheme. The tabulate results shows that

Table 2. Simulation results using $\tau = 0.01$, $t = 0.1$, $N^2 = 10$, and $\beta = 0.2$ for Test problem 2

		LMM		[29]	
	α	max(ε)	*RMS*	max(ε)	*RMS*
Crank-Nicolson	0.5	$7.8642 \cdot 10^{-3}$	$1.7654 \cdot 10^{-3}$	$1.649 \cdot 10^{-2}$	$5.152 \cdot 10^{-3}$
	0.75	$2.3956 \cdot 10^{-3}$	$9.3420 \cdot 10^{-4}$	$2.020 \cdot 10^{-2}$	$7.248 \cdot 10^{-3}$
	0.95	$1.6148 \cdot 10^{-3}$	$6.7500e \cdot 10^{-4}$	$2.406 \cdot 10^{-2}$	$1.114 \cdot 10^{-2}$
Implicit	0.5	$3.4386 \cdot 10^{-2}$	$7.5629 \cdot 10^{-3}$	$1.708 \cdot 10^{-2}$	$5.043 \cdot 10^{-3}$
	0.75	$5.6834 \cdot 10^{-3}$	$2.4142 \cdot 10^{-3}$	$2.099 \cdot 10^{-2}$	$6.711 \cdot 10^{-3}$
	0.95	$4.6410 \cdot 10^{-3}$	$2.0979 \cdot 10^{-3}$	$2.453 \cdot 10^{-2}$	$9.230 \cdot 10^{-3}$

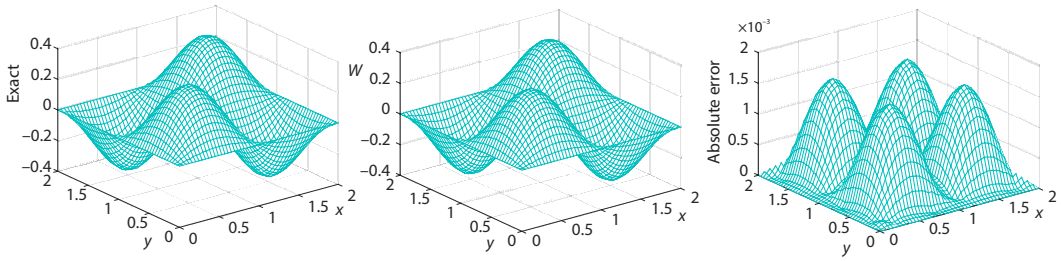

Figure 3. Simulation results using $\tau = 0.01$, $t = 1$, $\alpha = 0.75$, $\beta = 0.2$ and $N^2 = 20$ for Test problem 2

Table 3. Simulation results using $\tau = 0.01$, $\beta = 0.2$, spatial domain $[0, 2]^2$ and $N^2 = 10$ for Test problem 2

		Explicit		Crank-Nickolson		Implicit	
	t	max(ε)	*RMS*	max(ε)	*RMS*	max(ε)	*RMS*
$\alpha = 0.75$	0.2	1.2119×10^{-5}	5.6233×10^{-6}	1.4292×10^{-3}	6.7039×10^{-4}	2.6446×10^{-3}	1.2472×10^{-3}
	0.4	1.0352×10^{-5}	4.8033×10^{-6}	1.2086×10^{-3}	5.7048×10^{-4}	2.2373×10^{-3}	1.0620×10^{-3}
	0.6	8.6493×10^{-6}	4.0132×10^{-6}	1.0051×10^{-3}	4.7580×10^{-4}	1.8608×10^{-3}	8.8597×10^{-4}
	0.8	7.1812×10^{-6}	3.3320×10^{-6}	8.3190×10^{-4}	3.9457×10^{-4}	1.5402×10^{-3}	7.3483×10^{-4}
	1	5.9464×10^{-6}	2.7591×10^{-6}	6.8713×10^{-4}	3.2642×10^{-4}	1.2722×10^{-3}	6.0797×10^{-4}
$\alpha = 0.95$	0.2	2.2911×10^{-5}	1.0630×10^{-5}	6.5271×10^{-4}	3.2970×10^{-4}	1.2713×10^{-3}	6.4211×10^{-4}
	0.4	1.9471×10^{-5}	9.0344×10^{-6}	5.5633×10^{-4}	2.7990×10^{-4}	1.0843×10^{-3}	5.4545×10^{-4}
	0.6	1.6146×10^{-5}	7.4914×10^{-6}	4.6171×10^{-4}	2.3200×10^{-4}	8.9995×10^{-4}	4.5214×10^{-4}
	0.8	1.3330×10^{-5}	6.1852×10^{-6}	3.8141×10^{-4}	1.9150×10^{-4}	7.4345×10^{-4}	3.7321×10^{-4}
	1	1.0988×10^{-5}	5.0985×10^{-6}	3.1454×10^{-4}	1.5782×10^{-4}	6.1311×10^{-4}	3.0758×10^{-4}

explicit scheme produced better results as compared to Crank-Nicolson and implicit scheme. The LMM is testified on non-rectangular domains as shown in figs. 4-6. It is clear from these figures that the LMM gives good numerical results irrespective of the domains.

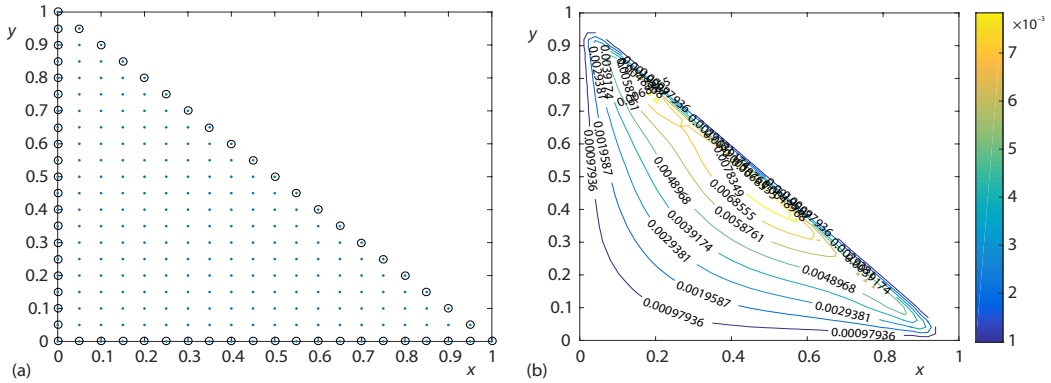

Figure 4. Computational domain (a) and absolute error (b) with $N^2 = 21$, $\tau = 0.001$, $t = 1$, $\alpha = 0.75$, and $\beta = 0.2$ for Test problem 2

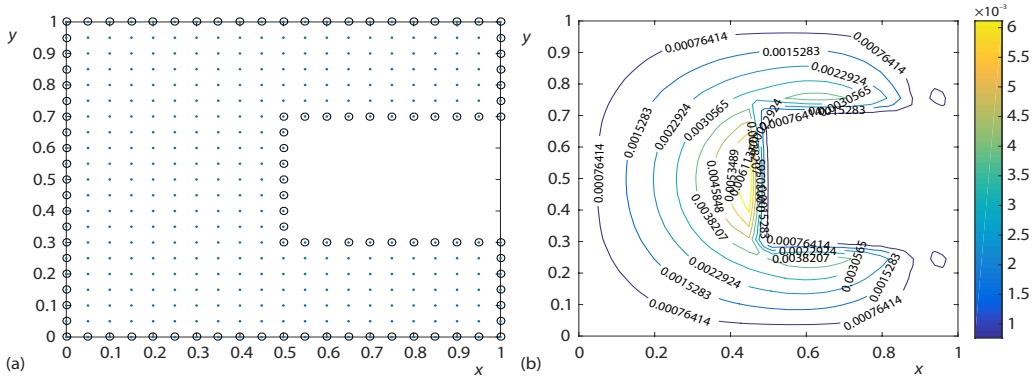

Figure 5. Computational domain (a) and absolute error (b) with $N^2 = 21$, $\tau = 0.001$, $t = 1$, $\alpha = 0.75$, and $\beta = 0.2$ for Test problem 2

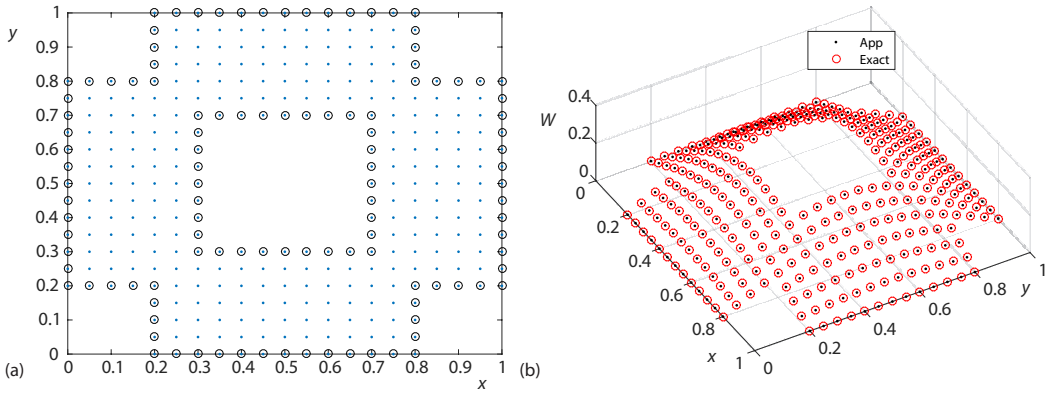

Figure 6. Computational domain (a) and solution (b) with $N^2 = 21$, $\tau = 0.001$, $t = 1$, $\alpha = 0.75$, and $\beta = 0.2$ for Test problem 2

Test problem 3

Consider the 3-D two term fractional-order diffusion eq. (1). For $a_1 = a_2 = \gamma = 1$ the exact solutions:

$$W(\bar{\mathbf{z}},t) = \sin(\pi x)\sin(\pi y)\sin(\pi z)\exp(-t), \quad t \geq 0(x,y,z) \in [0,1]^3 \tag{13}$$

The numerical results for in terms of max(ε) and RMS error norms for Test problem 3 are given in tab. 4 for different fractional order α and N. It can be seen from the table that the accuracy increases with increase in nodel points N to some extent. Also, tab. 5 indicate that the accuracy increases with the decrease in time step size τ. To testify the performance of the LMM on non-rectangular domains in 3-D case, the results are shown in figs. 7 and 8 which are self explanatory.

Table 4. Simulation results using $\tau = 0.01$, and $\beta = 0.2$ for Test problem 3

		$N^3 = 5$				$N^3 = 15$	
	α	max(ε)	*RMS*	max(ε)	*RMS*	max(ε)	*RMS*
$t = 0.5$	0.25	$9.0677 \cdot 10^{-3}$	$2.4847 \cdot 10^{-3}$	$5.8359 \cdot 10^{-3}$	$3.1153 \cdot 10^{-3}$	$4.4821 \cdot 10^{-3}$	$2.4230 \cdot 10^{-3}$
	0.5	$1.1407 \cdot 10^{-2}$	$3.8965 \cdot 10^{-3}$	$5.0931 \cdot 10^{-3}$	$2.8205 \cdot 10^{-3}$	$3.6906 \cdot 10^{-3}$	$2.0413 \cdot 10^{-3}$
	0.75	$9.8079 \cdot 10^{-3}$	$3.3734 \cdot 10^{-3}$	$3.3128 \cdot 10^{-3}$	$1.8649 \cdot 10^{-3}$	$2.3458 \cdot 10^{-3}$	$1.3205 \cdot 10^{-3}$
	0.95	$7.9310 \cdot 10^{-3}$	$2.5606 \cdot 10^{-3}$	$2.0002 \cdot 10^{-3}$	$1.1489 \cdot 10^{-3}$	$1.3851 \cdot 10^{-3}$	$8.0245 \cdot 10^{-4}$
$t = 1$	0.25	$5.5870 \cdot 10^{-3}$	$1.5276 \cdot 10^{-3}$	$3.5817 \cdot 10^{-3}$	$1.9206 \cdot 10^{-3}$	$2.7400 \cdot 10^{-3}$	$1.4920 \cdot 10^{-3}$
	0.5	$7.0947 \cdot 10^{-3}$	$2.4214 \cdot 10^{-3}$	$3.1382 \cdot 10^{-3}$	$1.7477 \cdot 10^{-3}$	$2.2619 \cdot 10^{-3}$	$1.2629 \cdot 10^{-3}$
	0.75	$6.1175 \cdot 10^{-3}$	$2.0932 \cdot 10^{-3}$	$2.0389 \cdot 10^{-3}$	$1.1537 \cdot 10^{-3}$	$1.4366 \cdot 10^{-3}$	$8.1582 \cdot 10^{-4}$
	0.95	$4.8866 \cdot 10^{-3}$	$1.5739 \cdot 10^{-3}$	$1.2357 \cdot 10^{-3}$	$7.0508 \cdot 10^{-4}$	$8.4490 \cdot 10^{-4}$	$4.9206 \cdot 10^{-4}$

Table 5. Simulation results using $t = 1$, $\alpha = 0.75$, and $\beta = 0.2$ for Test problem 3

$N^3 = 5$			$N^3 = 10$		$N^3 = 15$	
τ	max(ε)	*RMS*	max(ε)	*RMS*	max(ε)	*RMS*
0.1	$7.0399 \cdot 10^{-3}$	$2.0594 \cdot 10^{-3}$	$3.7033 \cdot 10^{-3}$	$2.0612 \cdot 10^{-3}$	$2.7287 \cdot 10^{-3}$	$1.5615 \cdot 10^{-3}$
0.01	$6.1175 \cdot 10^{-3}$	$2.0932 \cdot 10^{-3}$	$2.0389 \cdot 10^{-3}$	$1.1537 \cdot 10^{-3}$	$1.4366 \cdot 10^{-3}$	$8.1582 \cdot 10^{-4}$
0.001	$3.7268 \cdot 10^{-3}$	$1.1122 \cdot 10^{-3}$	$6.6573 \cdot 10^{-4}$	$3.6145 \cdot 10^{-4}$	$4.1150 \cdot 10^{-4}$	$2.3959 \cdot 10^{-4}$
0.0001	$2.8801 \cdot 10^{-3}$	$7.6295 \cdot 10^{-4}$	$2.8033 \cdot 10^{-4}$	$1.1662 \cdot 10^{-4}$	$1.1934 \cdot 10^{-4}$	$6.1069 \cdot 10^{-5}$

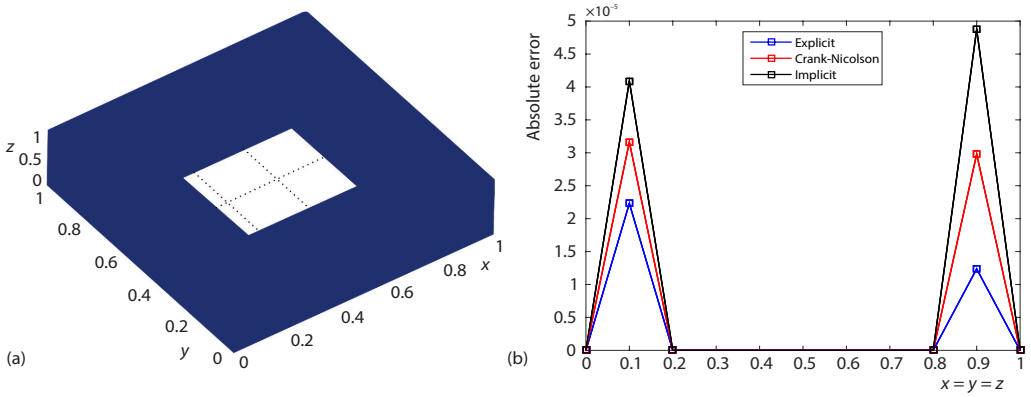

Table 7. Computational domain (a) and absolute error (b) with $N^3 = 11$, $\tau = 0.001$, $t = 1$, $\alpha = 0.95$, and $\beta = 0.2$ for Test problem 3

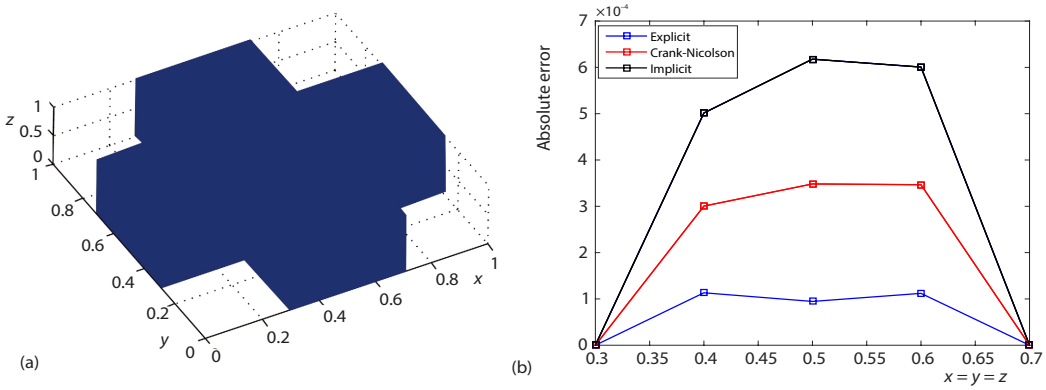

Table 8. Computational domain (a) and absolute error (b) with $N^3 = 11$, $\tau = 0.001$, $t = 1$, $\alpha = 0.95$, and $\beta = 0.2$ for Test problem 3

Conclusion

In this work, we have applied a LMM based on RBF as a modern powerful numerical method to investigate two term time fractional-order diffusion PDE models in 1-, 2- and 3-D cases. The time derivative part is defined and simplified in Liouville-Caputo sense and the scheme is constructed for $0 < \beta \leq \alpha < 1$. Test problems have been considered on rectangular and non-regular domains to check the accuracy of the proposed scheme. The numerical results are the evidence that the suggested LMM is a flexible interpolation method as it produce the coefficient matrix well-conditioned. In light of the current work we can say that the proposed technique is powerful and effective to find multi term time fractional PDE, so it can be also applied to a wide range of complex problems that occur in natural sciences and engineering.

Acknowledgment

This work was supported by National Natural Science Foundation of China (No. 71601072) and Key Scientific Research Project of Higher Education Institutions in Henan Province of China (No. 20B110006). B. Almohsen is Supported by Researchers Supporting Project number (RSP-2020/158), King Saud University, Riyadh, Saudi Arabia.

References

[1] Kelly, J. F., *et al*., Analytical Time-Domain Green's Functions for Power-Law Media, *Journal Acoust. Soc. Am*., *124* (2008), 5, pp. 286128-72
[2] Lubich, C., Discretized Fractional Calculus, *SIAM J. Math. Anal*, *17* (1986), 3, pp. 704-719
[3] Ahmad, H., Khan, T. A., Variational Iteration Algorithm i with an Auxiliary Parameter for the Solution of Differential Equations of Motion for Simple and Damped Mass-Spring Systems, *Noise Vib Worldw*, *51* (2020), 1-2, pp. 12-20
[4] Rafiq, M., *et al*., Variational Iteration Method with an Auxiliary Parameter for Solving Volterra's Population Model, *Non-linear Sci. Lett. A*, *8* (2017), 4, pp. 389-396.
[5] Bekir, A., *et al*., Applications of Fractional Complex Transform and G′/G-expansion method for time-fractional differential equations, *Journal Appl. Anal. Comput*., *6* (2016), Jan., pp. 131-144
[6] Ahmad, H., *et al*., Variational Iteration Algorithm-i with an Auxiliary Parameter for Solving Boundary Value Problems, *Earthline J. Math. Sci*., *3* (2020), 2, pp. 229-247
[7] Ahmad, I., *et al*., Local Meshless Differential Quadrature Collocation Method for Time-Fractional PDE, *Discrete Cont Dyn-S*, *13* (2020), 10, pp. 2641-2654
[8] Partohaghighi, M., *et al*., Ficitious Time Integration Method for Solving the Time Fractional Gas Dynamics Equation, *Thermal Science*, *23* (2019), Suppl. 6, pp. S2009-S2016
[9] El-Dib, Y., Stability Analysis of a Strongly Displacement Time-Delayed Duffing Oscillator Using Multiple Scales Homotopy Perturbation Method, *Journal Appl. Comput. Mech*., *4* (2018), 4, pp. 260-274
[10] Jena, R. M., *et al*., Dynamic Response Analysis of Fractionally Damped Beams Subjected to External Loads Using Homotopy Analysis Method, *Journal Appl. Comput. Mech*., *5* (2019), 2, pp. 355-366
[11] Li, C., Wang, Y., Numerical Algorithm Based on a Domian Decomposition for Fractional Differential Equations, *Comput. Math. with Appl*., *57* (2009), 10, pp. 1672-1681
[12] Bisheh-Niasar, M., Ameri, A. M., Moving Mesh Non-Standard Finite Difference Method for Non-Linear Heat Transfer in a Thin Finite Rod, *Journal Appl. Comput. Mech*., *4* (2018), 3, pp. 161-166
[13] Ahmad, H., Khan, T. A., Variational Iteration Algorithm-i with an Auxiliary Parameter for Wave-Like Vibration Equations, *Journal Low Freq Noise V A*, *38* (2019), 3-4, pp. 1113-1124
[14] Jassim, H. K., Baleanu, D., A Novel Approach for Korteweg-de Vries Equation of Fractional Order, *Journal Appl. Comput. Mech*., *5* (2019), 2, pp. 192-198
[15] Ahmad, H., Variational Iteration Method with an Auxiliary Parameter for Solving Differential Equations of the Fifth Order, *Non-Linear Sci. Lett. A*, *9* (2018), Mar., pp. 27-35
[16] Inc, M., *et al*., Modified Variational Iteration Method for Straight Fins with Temperature Dependent Thermaconductivity, *Thermal Science*, *22* (2018), Suppl. 1, pp. S229-S236
[17] Kilicman, A., *et al*., Analytic Approximate Solutions for Fluid-Flow in the Presence of Heat and Mass Transfer, *Thermal Science*, *22* (2018), Suppl. 1, pp. S259-S264
[18] Kucukarslan-Yuzbasi, Z., *et al*., On Exact Solutions for New Coupled Non-Linear Models Getting Evolution of Curves in Galilean Space, *Thermal Science*, *23* (2019), Suppl. 1, pp. S227-S233
[19] Akgul, A., *et al*., New Method for Investigating the Density-Dependent Diffusion Nagumo Equation, *Thermal Science*, *22* (2018), Suppl. 1, pp. S143-S152
[20] Inc, M., *et al*., Modified Variational Iteration Method for Straight Fins with Temperature Dependent Thermal Conductivity, *Thermal Science*, *22* (2018), Suppl. 1, pp. S229-S236
[21] Ahmad, I., *et al*., Numerical Simulation of Partial Differential Equations Via Local Meshless Method, *Symmetry*, *11* (2019), 257
[22] Oguntala, G., Abd-Alhameed, R., Thermal Analysis of Convective-Radiative Fin with Temperature-Dependent Thermal Conductivity Using Chebychev Spectral Collocation Method, *Journal Appl. Comput. Mech*., *4* (2018), 2, pp. 87-94
[23] Wendland, H., *Approximation Scattered Data*, Press Cambridge University, Cambridge, UK, 2005
[24] Ahmad, I., *et al*., An Efficient Local Formulation for Time-Dependent PDE, *Mathematics*, *7* (2019), 216
[25] Siraj-ul-Islam, Ahmad, I., A Comparative Analysis of Local Meshless Formulation for Multi-Asset Option Models, *Eng. Anal. Bound. Elem.*, *65* (2016), Apr., pp. 159-176
[26] Ahmad, I., *et al*., Numerical Simulation of PDE by Local Meshless Differential Quadrature Collocation Method, *Symmetry*, *11* (2019), 394
[27] Caputo, M., Linear Models of Dissipation whose Q is almost Frequency Independent-II, *Geophys. J. Int*., *13* (1967), 5, pp. 529-539

[28] Qiao, L., Xu, D., Orthogonal Spline Collocation Scheme for the Multi-Term Time-Fractional Diffusion Equation, *Int. J. Comput. Math*., *95* (2018), 8, pp. 1478-1493
[29] Hussain, M., Haq, S., Weighted Meshless Spectral Method for the Solutions of Multi-Term Time Fractional Advection-Diffusion Problems Arising in Heat and Mass Transfer, *Int. J. Heat Mass Transf*., *129* (2019), Feb., pp. 1305-1316

Paper submitted: April 15, 2020
Paper revised: May 29, 2020
Paper accepted: June 1, 2020

© 2020 Society of Thermal Engineers of Serbia
Published by the Vinča Institute of Nuclear Sciences, Belgrade, Serbia.
This is an open access article distributed under the CC BY-NC-ND 4.0 terms and conditions